Satellite structure in the argon valence shell by electron-momentum spectroscopy

I. E. McCarthy, R. Pascual, P. Storer, and E. Weigold
Electronic Structure of Materials Centre, School of Physical Sciences, The Flinders University of South Australia, Bedford Park, South Australia 5042, Australia
(Received 7 March 1989)

Momentum distributions and spectroscopic factors are obtained in a high-resolution study of argon at 500, 1000, and 1500 eV by electron-momentum spectroscopy. The shapes and relative magnitudes of the 1500-eV cross sections are in excellent agreement with the results of a distorted-wave impulse approximation calculation. The final states belonging to the $^2S^e$ and $^2P^o$ manifolds are identified and their spectroscopic factors (pole strengths) are obtained. These are found to be independent of energy and momentum in the range 0.1–1.9 a.u. within experimental error, although some momentum dependence is observed for the spectroscopic factor leading to the $4s\ ^2S$ ion state due to initial-state correlations. The first momentum profiles for excited states belonging to the $^2P^o$ and $^2D^e$ manifolds are obtained. The latter are entirely due to initial-state correlations. Comparison is made with several many-body calculations. The data show the importance of core quadrupole (^1D) excitations in describing electron correlations in both the initial Ar ground state and in the final ionic states.

I. INTRODUCTION

The relative intensity of the satellite structure observed in the valence binding energy spectrum of argon has been the subject of some controversy.[1–15] Much of this has focused on the $3s$ satellite structure, where inconsistencies appear to exist between photoelectron spectroscopy (PES) measurements at intermediate photon energies[12–15] and earlier x-ray PES measurements at higher energies.[16] There are also inconsistencies between the PES and the electron-momentum spectroscopy (EMS) data, the latter[1,3,17–23] being consistent among each other, giving satellite intensities and structure information independent of the incident energy. In general, the PES measurements are quite energy dependent, and measure a higher pole strength for the main $3s^{-1}$ transition (that is, the transition leading to the $3s3p^6$ ion state at a separation energy of 29.3 eV) than obtained in the EMS measurements. Part of this problem is the difficulty inherent in the PES measurement of measuring the strength in the continuum (i.e., double-ionization region).[2] In EMS the measurement of the continuum strength presents no difficulty, since background subtraction does not depend on the presence or absence of peaks. Thus in PES measurements it is difficult to observe the total transition strength, and the relative intensities of a few peaks are all that are generally reported.

Both EMS and high-energy PES can be used to study initial- and final-state correlation effects in atoms and molecules. The kinematics of these two experiments are, however, quite different. EMS measurements are performed at low recoil momenta ($p \leq 1.5$ a.u.), whereas the high-energy PES experiments are performed at high recoil momenta ($p \sim 3$–10 a.u.). In other words, EMS probes the low momentum components of the target wave fucntion which is dominated by the large-r region, whereas PES probes the very-high-momentum tail of the wave function dominated by the regions close to the nuclei. Further, in EMS the momentum of the target electrons probed is independent of the incident energy, whereas in PES it depends directly on the energy, since it is proportional to the square root of the outgoing electron energy. Therefore in PES different satellites at the same photon energy, or the same satellite at different photon energies, correspond to different parts of the momentum-space wave functions and probability distributions, i.e., have different cross sections.

It is therefore not surprising that there are differences between EMS and PES spectroscopic strengths. The spectroscopic strengths or pole strengths for any transition at any given momentum should be independent of incident energy or ejected energy. Any purely structural property, such as spectroscopic strengths, should not depend on the energies of the particles. PES transition intensities are, however, intrinsically energy dependent. This is because as the energy varies, the momentum component of the wave function that is probed is varied. As well as the momentum probability distribution changing, it is well known[1,19] that if initial-state correlation effects play a role, the spectroscopic factor must be momentum dependent. Further, at the low energies where many PES experiments are carried out (<200 eV, say), the emitted electrons, which come from the strong part of the potential (high p), cannot be considered as plane waves, thus making the calculation of the orbital and continuum matrix elements difficult and energy dependent. In EMS it is possible to fix the momentum as the energy is changed and to measure directly energy-independent structure information.

In the present work we report some detailed measurements at 500, 1000, and 1500 eV. At each energy, in addition to obtaining spectroscopic strengths for the various $3s^{-1}$ transitions, we observe several $3p^{-1}$ satellite lines, the first clear observation of this in EMS. The

$3p^{-1}$ satellites have a completely different momentum dependence to the $3s^{-1}$ satellites and are therefore simple to identify. We also observe, for the first time, excitation of ^2D final states due to initial-state correlations. We report the measured momentum profiles at 1500 eV for various transitions, and show that the dominant $3p^{-1}$ and $3s^{-1}$ transitions can be fully understood on the basis of the distorted-wave impulse approximation. That is, the measured shapes and relative cross sections are completely given by the theoretical calculation.

II. THEORETICAL BACKGROUND

In the present work noncoplanar symmetric kinematics is employed, that is, the outgoing energies E_1 and E_2 are equal, the two emitted electrons making equal polar angles $\theta=45°$ with respect to the incident electrons of energy $E_0=\varepsilon_f+E_1+E_2$, where ε_f is the binding or electron separation energy. The ion recoil momentum $\mathbf{p}=\mathbf{p}_0-\mathbf{p}_1-\mathbf{p}_2$ is varied by varying the out-of-plane azimuthal angle $\phi=\pi-\phi_1-\phi_2$. The experimental method is the same as the one outlined in Refs. 23 and 24.

The EMS differential cross section is given by[1,19]

$$\frac{d^5\sigma}{d\hat{\mathbf{p}}_1 d\hat{\mathbf{p}}_2 dE_2}=(2\pi)^4\frac{p_1 p_2}{p_0}f_{e\text{-}e}G_f(p)\ , \tag{1}$$

where the electron-electron collision factor f_{e-e} is the half-off-shell (to allow for the binding energy) Mott scattering cross section averaged over electron-spin degeneracies. In the noncoplanar symmetric geometry the collision and kinematical factors are essentially independent of the angle ϕ and the cross section is proportional to the structure factor $G_f(p)$,[1,18] which for incident and outgoing plane waves (the plane-wave impulse approximation PWIA) is given by

$$G_f(p)=(2J_0+1)^{-1}\sum_{M_0,M_f}|\langle \mathbf{p}\Psi_f{:}J_fM_f|\Psi_0{:}J_0M_0\rangle|^2\ , \tag{2}$$

where the sum over final electronic degeneracies and an average over initial-state electronic degeneracies are taken, and $|\Psi_0\rangle$ and $|\Psi_f\rangle$ are the N and $N-1$ electron initial and final states, respectively (note that $|\Psi_f\rangle$ need not be bound). The notation used in the bra vector of (2) indicates the $(N-1)$-electron–ion state f and an electron in a plane-wave state with momentum $\mathbf{p}$. By measuring the cross section as a function of $\mathbf{p}$ it is possible to measure the square of the (one electron) overlap function $\langle\Psi_f|\Psi_0\rangle$ in momentum space. This is the probability that the observed ion state $|\Psi_f\rangle$ is obtained by annihilating an electron of momentum $-\mathbf{p}$ and spin coordinate σ in the target state $|\Psi_0\rangle$. In the second quantized notation the operator that annihilates such an electron is $\sum_{j,\alpha,m}\phi^j_{\alpha m}(\mathbf{p},\sigma)a^j_{\alpha m}$. The function $\phi^j_{\alpha m}$ is the single-particle orbital in momentum-spin space for total angular momentum j with projection m. The remaining quantum numbers are denoted by α (e.g., principal quantum number for an atomic orbital). The radial factor of $\phi^j_{\alpha m}(\mathbf{p},\sigma)$ is denoted $\phi^j_\alpha(p)$. The structure factor (2) can then be written[1,19]

$$G_f(p)=(2J_0+1)^{-1}\sum_{j,\alpha,\beta}\phi^j_\alpha(p)\phi^j_\beta(p)\langle\Psi_0||(\mathbf{a}^j_\alpha)^\dagger||\Psi_f\rangle\cdot\langle\Psi_f||\mathbf{a}^j_\beta||\Psi_0\rangle\ . \tag{3}$$

The dot product in (3) denotes the scalar product of tensor operators

$$\mathbf{a}^j_\alpha\cdot\mathbf{a}^j_\beta=\sum_m(a^j_{\alpha m})^\dagger a^j_{\beta m}\ . \tag{4}$$

There is a manifold of states $|\Psi_f\rangle$ that contain the one-hole configuration resulting from the annihilation of an electron in the characteristic orbital $\phi^j_\alpha(p)$ in $|\Psi_0\rangle$. One can define the manifold structure factor $W_{j\alpha}(p)$ by summing over all final states belonging to the manifold characterized by $j\alpha$

$$W_{j\alpha}(p)=\sum_{f\in j\alpha}G_f(p)$$
$$=(2J_0+1)^{-1}\sum_{k,\mu,\nu}\phi^k_\mu(p)\phi^k_\nu(p)\langle\Psi|(\mathbf{a}^k_\mu)^\dagger\cdot\mathbf{a}^k_\nu|\Psi_0\rangle\ . \tag{5}$$

This sum is dominated by the term $k=j$, $\mu=\nu=\alpha$, hence the manifold structure factor is labeled by j,α. The last factor is the target ground-state density matrix obtained by a structure calculation and it can be sensitive to details in different many-body calculations of the ground state $|\Psi_0\rangle$.

The spectroscopic factor or pole strength $S_{f,j\alpha}(p)$ for the one-hole manifold $j\alpha$ is given by

$$G_f(p)=S_{f,j\alpha}(p)W_{j\alpha}(p)\ . \tag{6}$$

It is obvious that the spectroscopic factors obey the sum rule

$$\sum_{f\in j\alpha}S_{f,j\alpha}(p)=1\ . \tag{7}$$

It is important to note the spectroscopic factors can depend on p, where p is the momentum of the ionized electron in the target state. The simplest approximation to the photoelectron cross section, involving the plane-wave and sudden approximations, contains the same factor. It is often confusingly called shake-up theory in PES.

For closed-shell targets it is often reasonable to make the target Hartree-Fock approximation (THFA) in which $|\Psi_0\rangle=|\Phi_0\rangle$ is the Hartree-Fock configuration for the target. In this case the structure factor simplifies to

$$G_f(p)=(2j+1)S_{f,j\alpha}[\phi^j_\alpha(p)]^2 , \quad (8)$$

and the spectroscopic factor is now independent of momentum. It is only when there are no correlations in the initial state that the spectroscopic factor is strictly independent of momentum. The spectroscopic factor in this THFA is simply the probability that $|\Psi_f\rangle$ consists of a hole in $|\Phi_0\rangle$ with quantum numbers j,α.

The noncoplanar symmetric EMS cross section at a given energy is directly proportional to the structure factor [Eqs. (3), (6), and (8)] and this depends on both the spectroscopic factors, which give the relative intensities of the lines in a given manifold, and the momentum space wave functions of the orbital(s) involved.

Thus for atoms the cross sections for knocking out electrons from orbitals with $l>1$ are zero at $p=0$ (except for the effects of finite momentum resolution), whereas the cross sections for the $l=0$ manifolds have a maximum value at $p=0$. In EMS spectroscopy it is therefore easy to measure the s manifold cross sections, say, the $3s$ manifold in Ar^+, without interference from other manifolds, such as the $3p$ in Ar^+. Similarly, the $3p$ cross section peaks at about $p=0.65$ a.u., where the $3s$ cross section has dropped to about one-third of its maximum value.

It is not necessary to assume that the free electrons are plane waves, although the higher the energy the better this approximation becomes. Thus in the distorted-wave impulse approximation (DWIA) we replace the structure factor (2) by the distorted structure factor.[19] In the THFA this is for an atomic target simply given by

$$G_f(p)=S_{f,j\alpha}\sum_m |\langle \chi^{(-)}(\mathbf{p}_1)\chi^{(-)}(\mathbf{p}_2)|\phi^j_{\alpha m}\chi^{(+)}(\mathbf{p}_0)\rangle|^2 , \quad (9)$$

where $\chi^{(\pm)}(\mathbf{p})$ are elastic scattering wave functions for electrons in the appropriate equivalent local static exchange potentials.

III. EXPERIMENTAL ARRANGEMENT

The noncoplanar symmetric coincidence spectrometer and associated equipment has been described in some detail previously.[3,23,24] Binding-energy spectra spanning different energy intervals were measured at each of a number of out-of-plane azimuthal angles $\phi=\pi-\phi_1-\phi_2$. The data were obtained in a binning mode in which the entire spectrum was windowed across the microchannel plates, so that each part of the spectrum was collected at every angle for an equal time on each part of the channel plates. In any run the binding-energy spectra at the different angles were scanned repeatedly over the whole angular range. Momentum distributions were extracted from sequentially obtained angularly correlated binding energy spectra in order to maintain relative normalizations. A Gaussian fitting program was used to fit the peaks, the experimental energy resolutions being determined by accurate measurements of the $He(e,2e)He^+$ ground-state transition. The operating conditions were $E_0=E+\varepsilon_f$, with $E_1=E_2=E/2$ and $\theta_1=\theta_2=45°$. Runs were taken at total energies E of 500, 1000, and 1500 eV. The angular resolution was about 1° and the energy resolution varied with each run from 1.1 eV at 500 eV to 1.3 and 1.6 eV at 1500 eV. The energy resolution was primarily determined by the space-charge-induced energy spread of the incident electron beam.

Two runs were carried out at 500 eV, the first at $\phi=0°$ and 10° and the second at the angles 1°, 6°, 11°, 14°, 20°, 30°, and 36°. At 1000 eV spectra were taken over the separation energy range 25–55 eV at $\phi=0°$, 4°, 8°, and 12°, and at 1500 eV there were several independent runs over the angular range +10° to −25°.

IV. RESULTS AND DISCUSSION

A. Binding-energy spectrum

The binding-energy spectrum of Ar in the region 25–55 eV is shown in Fig. 1 for a total energy of 500 eV and with the out of plane azimuthal angles $\phi=0°$ and $\phi=10°$. At $\phi=0°$ the momentum p ranges from 0.17 a.u. at the binding energy of the first peak ($\varepsilon_f=29.24$ eV) to 0.29 a.u. for $\varepsilon_f=50$ eV. At 10° the corresponding momenta are 0.56 and 0.60 a.u., respectively. The spectra shown in Fig. 1 are considerably better resolved than those in earlier published works,[17–21] the exception being the statistically quite limited 300 eV spectrum of Williams,[22] which was taken with an energy resolution of about 0.8 eV. The spectra in Fig. 1 show some satellites not previously resolved in EMS and one not previously observed in PES.

For the sake of clarity, the $3p^{-1}$ ground-state transition is not included in the spectra. At $\phi=0°$, i.e., at low momentum, the $3p$ ground-state cross section is only 40% of that for the $3s^{-1}$ transition at 29.24 eV, whereas at $\phi=10°$ (i.e., $p\sim0.56$ a.u.) its cross section is about four times that of the 29.24 eV transition. Thus any reasonable $3p^{-1}$ satellite intensity in the range 25–55 eV should be noticeable in Fig. 1 by peaks which are much stronger at $\phi=10°$ than at $\phi=0°$. Peak 5 at 37.15 eV is obviously such a case and peak 3 at 35.64 eV is also a possible case. Peak 7 at 39.56 eV also has considerable strength at $\phi=10°$. The relative intensities of the peaks in Fig. 1, as well as that of the ground-state $3p^{-1}$ transition, are given in Table I. The intensities are relative to the $\phi=3s^{-1}$ transition at 29.24 eV. The table also gives the separation energies and final-state assignments.

Peak 2 at 34.20±0.08 eV does not correspond to a final state with $^2P^o$ or $^2S^e$ symmetry which must occur if, respectively, a $3p$ or $3s$ electron is ionized in the THFA. There is, however, a state of ^2D symmetry at 34.20 eV in Ar^+.[25] Excitation of this state can only occur if there are suitable correlations in the argon ground state. The state at 34.20 eV has been assigned the configuration $3s^23p^4(^1D)4s(^2D)$ by Moore.[25] The corresponding ground-state configuration, which much be even parity and coupled to $J=0$, has to be $3s^23p^4(^1D)4s3d$ $(^1S,J=0)$, the core having a quadrupole two-hole excitation, the two particles going into a $4s$ and $3d$ excited orbital. Knockout of the $3d$ electron would then lead to the state at 34.20 eV, whereas the knock-out of the $4s$ electron would lead to the $3s^23p^4(^1D)3d(^2S)$ state at 38.6 eV. Excitation of this state (peak 6) is observed to be very

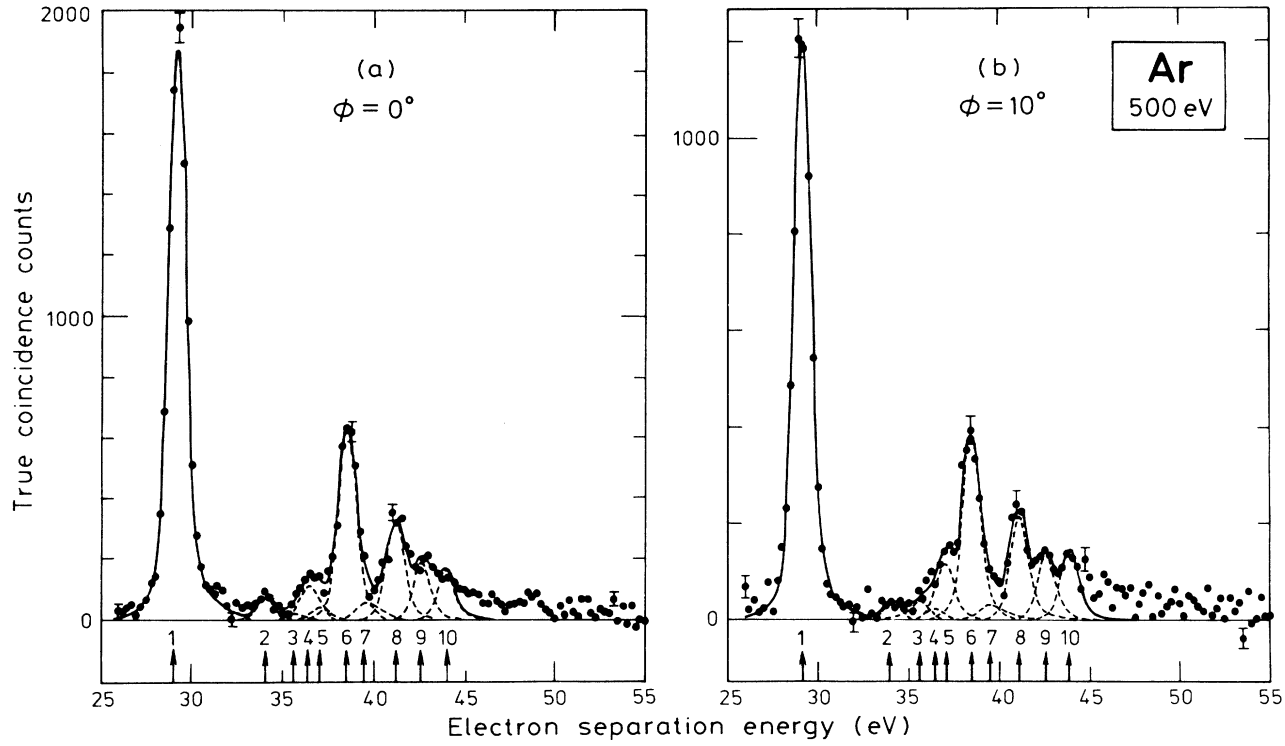

FIG. 1. 500-eV noncoplanar symmetric EMS separation energy spectra at $\phi=0°$ ($p\sim0.2$ a.u.) and $\phi=10°$ ($p\sim0.58$ a.u.). The curves show the fitted spectra using the known energy resolution. The assignments for the peaks 1–10 are given in Table I.

strong, but the major contribution to its strength is from final-state correlation effects,[1–20] the state containing a significant 3*s*-hole contribution and can therefore be reached by direct 3*s* ionization.

The intensity of peak 3 at 35.64 eV is very small, the cross section at $\phi=10°$ being higher than that at $\phi=0°$, which means that it cannot be a 3*s* satellite and must be a 3*p* satellite due to initial- or final-state correlation effects or relaxation effects. There is a $^2P^o$ state at 35.60 eV with configuration $3s^23p^4(^3P)4p$ that could certainly be excited due to relaxation and or correlation effects. The initial- and final-state configuration-interaction (CI) calculation of Mitroy *et al.*[5] predicts a $3p^{-1}$ strength leading to this state of 0.002. Dyall and Larkins[26] in their CI calculation obtain a similar result. The 500-eV 10° data in Table I show that the maximum $3p^{-1}$ strength to this

TABLE I. Peak energies and relative intensities in the 500-eV spectra shown in Fig. 1 The intensities are relative to a value of 100 for the 29.24-eV transition at $\phi=0°$. The error in the last significant figure is shown in parentheses. The momentum p depends on the binding energy, the lower value is for $\varepsilon=29.24$ eV, the upper for $\varepsilon=40$ eV.

Peak	ε_f (eV)	Final state	$\phi=0°$ $p=0.17$–0.23 a.u.	$\phi=10°$ $p=0.56$–0.60 a.u.
	15.76	$3s^23p^5\,^2P^o$	45(5)	250(20)
1	29.24	$3s3p^6\,^2S$	100	63.2(8)
2	34.20	$3s^23p^4(^1D)4s\,^2D$	4.1(3)	1.8(3)
3	35.6	$3s^23p^4(^3P)4p\,^2P^o$	1.2(3)	2.0(3)
4	36.52	$3s^23p^4(^1S)4s\,^2S$	5.7(4)	1.1(4)
5	37.15	$3s^23p^4(^1D)4p\,^2P^o$	2.3(4)	6.0(6)
		$3s^23p^4(^1D)3d\,^2D$		
6	38.60	$3s^23p^4(^1D)3d\,^2S$	33.0(6)	19.9(6)
7	39.56	$3s^23p^4(^1S)4p\,^2P^o$	2.9(4)	1.6(4)
		$3s^23p^4(^3P)4d\,^2D$		
8	41.21	$3s^23p^4(^1D)4d\,^2S$	17.0(5)	11.0(5)
9	42.67	$3s^23p^4(^1D)5d\,^2S$	9.6(6)	6.2(6)
10	44.0		8.1(6)	6.7(6)

state is 0.01 at $p \sim 0.58$. There is also a $^2D^o$ state at 35.44 eV with the same configuration. Such a state could be excited in the weak-coupling approximation if the corresponding configuration $3s^2 3p^4(^3P)4p^2$ $(J=0)$ plays a significant role in the argon ground state. The resulting $4p$ momentum distribution would peak at a lower value of momentum than the $3p$.

Peak 4 at 36.52 eV again belongs to the ^2S manifold, the cross section at $\phi=0$ being much larger than at $\phi=10°$. The final state is $3s^2 3p^4(^1S)4s\ ^2S$, and both relaxation effects and correlations lead to its excitation.

Peak 5 at 37.15 eV again has a much larger cross section at $\phi=10°$ ($p=0.58$ a.u.) than at $\phi=0°$ ($p=0.22$ a.u.). It therefore cannot be a $3s$ satellite. There are two possible final states in the energy region of interest, namely, the $(^1D)4p\ ^2P^o$ state at 37.11 eV belonging to the $3p$ manifold and the $(^1D)3d\ ^2D$ state at 37.18 eV belonging to the $3d$ manifold. This latter state can only be excited if ground-state correlations lead to significant $3s^2 3p^4(^1D)3dnl$ $(J=0)$ ^1S configurations in the ground state. Mitroy *et al.*[5] find in their CI calculation of the generalized overlap amplitude [Eq. (2)] that there should be significant excitation of the $^2P^o$ state due to $3p$ ionization, the strength relative to the ground-state transition at $p=0.70$ a.u. being 0.013, compared with the present result of 0.032. Mitroy *et al.* calculate that the total strength for the $^2D^e$ correlation satellites at $p \approx 0.25$ a.u. should be only of the order of 0.4% of the $3s$ 29.24-eV cross section at $p \sim 0$. Dyall,[27] on the other hand, finds in his CI calculation that the cross section for exciting the $(^1D)3d\ ^2D$ ion state should be much higher, being about 5% of the $\phi=0°$ $3s$ 29.24-eV cross section at $p=0.25$ a.u. Given the very small cross section at $\phi=0°$ ($p=0.22$ a.u.) for this peak, the $(^1D)3d\ ^2D$ ion state could contribute only a very small part of the observed strength for this peak. We will return to this later when discussing the momentum distributions.

The remaining peaks all obviously belong to the $3s$ manifold, except for peak 7 at 39.56 eV. This peak, which has been observed in the recent high-resolution low-medium energy PES studies[12–14] and in the high-resolution x-ray photoelectron spectroscopy (XPS) study,[15] must arise from excitation of either the $(^1S)4p\ ^2P^o$ state at 39.57 eV belonging to the $^2P^o$ manifold, and or the excitation of the $(^3P)4d\ ^2D$ state at 39.64 eV belonging to the $^2D^e$ manifold. In the PES studies the satellite was assigned to the $(^1S)4p\ ^2P^o$ state.[14,15] The present data give an upper limit of 0.01 for the spectroscopic factor of this state, which compares with the value of 0.003 calculated by Dyall and Larkins[26] and 0.002 by Mitroy *et al.*[5]

B. Momentum distributions

Binding-energy spectra similar to those shown in Fig. 1 were also taken over a range of out-of-plane azimuthal angles at each total energy. Since each part of each spectrum at every angle was scanned sequentially for an equal

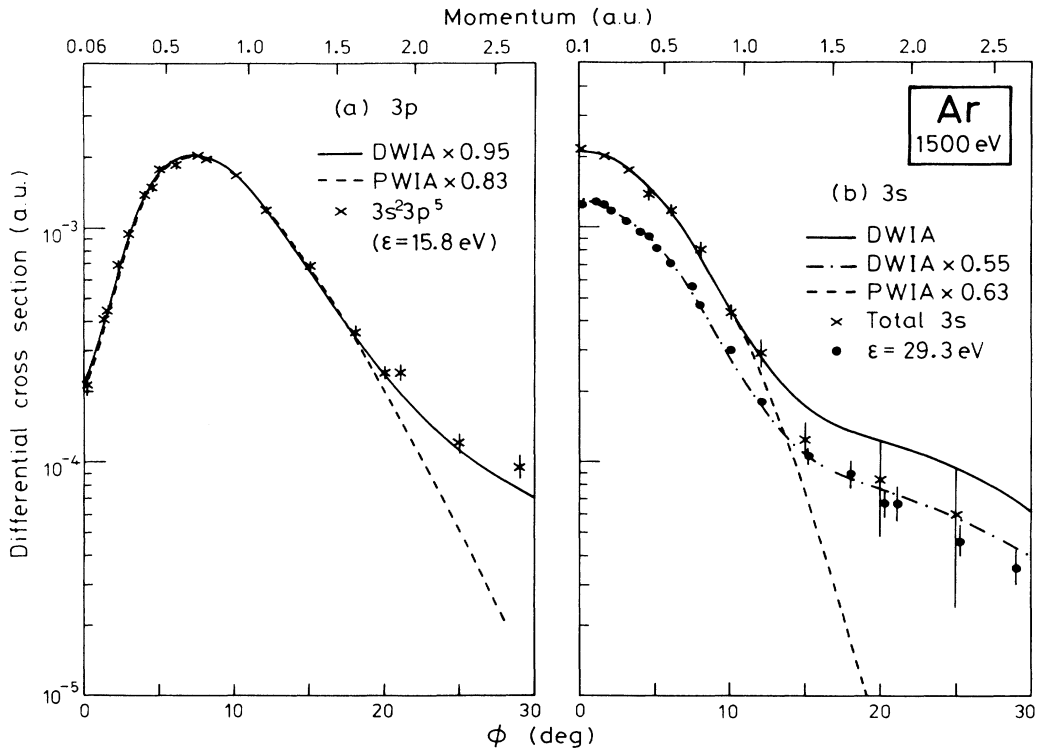

FIG. 2. 1500-eV noncoplanar symmetric angular correlations for the ground state (15.8 eV), first excited state (29.3 eV), and total ^2S manifold compared with the DWIA and PWIA cross sections using HF $3p$ and $3s$ wave functions. All of the data have been normalized by fitting the measured ground-state transition to 0.95 times the $3p$ DWIA cross section.

time, each run consisting of many scans, the spectra can be used to obtain the cross sections to selected final ion states relative to each other as a function of ϕ or momentum through the relationship

$$p=|\mathbf{p}_1+\mathbf{p}_2-\mathbf{p}_0|$$
$$=[(2p_1\cos\theta-p_0)^2+4p_1^2\sin^2\theta\sin^2\phi/2]^{1/2}\ . \qquad (10)$$

The 1500-eV noncoplanar symmetric $(e,2e)$ cross sections for the ground-state $3p^{-1}$ transition at 15.8 eV, for the ^2S manifold, (i.e., the integrated $3s^{-1}$ transition strength over the region $\varepsilon=29.24-55$ eV), as well as for the $3s^{-1}$ transition at 29.24 eV, are shown in Fig. 2 compared with various calculated distributions. The solid line is the DWIA cross section obtained using the THFA and the distorted-wave structure factor (9). The $3p$ and $3s$ HF wave functions of Clementi and Roetti[28] are used in the calculations. The measured angular correlations are not absolute, but relative normalizations are maintained. The measured cross sections are normalized to the DWIA by fitting the measured cross section at $p=0.5$ a.u. in the $3p$ ground-state transition to the DWIA value at that point. Nearly all of the $3p$ strength goes to the ground state transition. This can be seen from Table I and is supported by the detailed CI calculations of the overlap function by Mitroy *et al.*,[5] who find in their calculation of the $3p$ manifold that the spectroscopic factor for the ground-state transition is 0.995 at $p=0.12$ and 0.972 at $p=0.70$. We find in the present measurements that the spectroscopic factor for the $3p$ ground-state transition is 0.95 ± 0.02, and we have taken this value in normalizing the data. Therefore the DWIA-HF $3p$ cross section, which gives the cross section for the whole $3p$ manifold, has been multiplied by 0.95.

Figure 2 shows that the DWIA cross section for the $3s$ manifold is in excellent agreement with the measured $3s$ manifold cross section both in shape and in magnitude. This shows that all the $3s$ strength has been observed in the measurements over the separation energy region 29–55 eV. The shape of the 29.24-eV transition is also in excellent agreement with the DWIA calculation, as is its magnitude when the calculated manifold cross section is multiplied by the factor 0.55. This implies that the spectroscopic strength to this state should be 0.55 (see Table II). Also shown in Fig. 2 are the plane-wave impulse approximation cross sections for the corresponding transitions. These are simply proportional to $S_{f,j\alpha}[\phi_\alpha^j(p)]^2$, as shown by expressions (1) and (8). The shapes of the cross sections are very well described by the PWIA, i.e., by $[\phi_\alpha^j(p)]^2$, for momenta below 1.5 a.u. Above this momentum, where the cross section is very small, the distortion of the electron waves has a significant effect on the shape of the cross section. Although giving an excellent description of the momentum distribution at low momentum, the PWIA does, however, overestimate the $3s$ manifold cross section relative to that for the $3p$ manifold. This is due to the neglect of distortion and absorption in the PWIA, such effects being more important for the more tightly bound inner valence $3s$ orbital.

Mitroy *et al.*[5] carried out a detailed CI calculation of the full overlap function and the ground-state density ma-

TABLE II. Relative spectroscopic factors for the ^2S manifold of Ar II determined from relative $(e,2e)$ cross sections at different azimuthal angles ϕ at 500, 1000, and 1500 eV. The average momentum p probed at that angle is also given. The one standard deviation error in the last significant figure is given in parentheses.

Dominant configuration	E (eV) / ϕ / p (a.u.) / ε (eV)	500 eV 0°	6°	10°	14°	20°	30°	36°	1000 eV 0°	4°	8°	12°	1500 eV 0°	4.5°	8°	12°
		0.22	0.4	0.6	0.77	1.07	1.6	1.9	0.15	0.34	0.62	0.92	0.14	0.44	0.75	1.1
$3s3p^6\,^2S$	29.23	0.530(2)	0.54(2)	0.550(20)	0.52(3)	0.51(5)	0.53(7)	0.59(8)	0.56(1)	0.55(1)	0.56(2)	0.55(2)	0.56(1)	0.55(1)	0.53(2)	0.53(3)
$3s^23p^4(^1S)4s$	36.51	0.042(8)	0.01(1)	0.023(8)	0.04(2)	−0.03(4)	0.03(4)	0.02(4)	0.03(1)	0.02(1)	0.01(2)	0.00(2)	0.02(1)	0.01(1)	0.02(1)	0.00(2)
$3s^23p^4(^1D)3d$	38.59	0.176(14)	0.15(1)	0.163(13)	0.15(1)	0.16(2)	0.11(3)	0.15(3)	0.17(1)	0.17(1)	0.18(2)	0.12(3)	0.15(2)	0.16(1)	0.16(2)	0.15(2)
$3s^23p^4(^1D)4d$	41.27	0.087(7)	0.08(1)	0.090(12)	0.08(1)	0.09(2)	0.08(2)	0.07(2)	0.08(1)	0.09(1)	0.08(2)	0.07(2)	0.07(1)	0.08(1)	0.07(1)	0.09(2)
$3s^23p^4(^1D)5d,6d$	42–43.6	0.052(14)	0.12(2)	0.100(20)	0.11(2)	0.13(3)	0.11(3)	0.14(4)	0.09(2)	0.10(2)	0.11(2)	0.10(3)	0.07(1)	0.08(1)	0.08(2)	0.08(2)
Continuum	43.6–55	0.113(20)	0.11(2)	0.074(30)	0.12(2)	0.15(3)	0.13(3)	0.04(4)	0.09(2)	0.11(2)	0.09(2)	0.19(3)	0.12(1)	0.12(2)	0.14(2)	0.15(2)

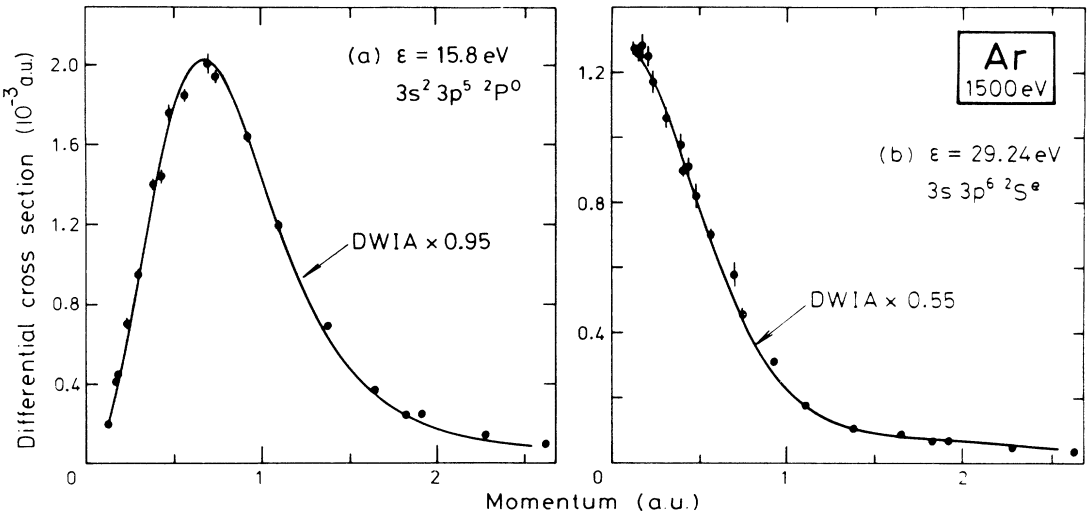

FIG. 3. Momentum profiles for the ground- and first excited-state transitions compared with the calculated cross sections multiplied by the respective spectroscopic factors.

trix to determine the momentum distributions for the $l=0$, 1, and 2 manifolds using Eqs. (2) and (5). They find that the $l=0$ manifold distribution $W_0(p)$ has essentially the same shape and magnitude as that given by the $3s$ Ar HF wave function, the only difference being a slight increase in the total strength at $p=0$ a.u. (by some 4%) due to the large value of $\phi_{4s}(p)$ at the origin, there being some small $4s$ contribution due to correlations in the ground-state wave function. Similarly, the effects of correlations on $W_1(p)$ were found to be very small, the shape and magnitude being very similar to the HF $3p$ momentum distribution. $l=2$ transitions leading to $^2D^e$ correlation satellites can only arise from d-wave correlations in the ground state. Mitroy *et al.* found that the major effect of the d-wave correlations was at large p (~ 1.2 a.u.), although there was a peak at low momentum centered at $p=0.25$ a.u., with an intensity of about 2% of the peak $3s$ intensity. Dyall,[27] on the other hand, found that the $l=2$ manifold cross section should be sharply peaked at $p\sim 0.25$ a.u. and have a value of almost a factor of 10 higher than that given by Mitroy *et al.* The difference in the calculations is that Mitroy *et al.* included special pseudonatural correlating orbitals in their calculations, these orbitals (e.g. $\overline{3d}$) being localized in the same region of space as the $3s$ and $3p$ orbitals. They found that the contracted $\overline{3d}$ orbital was much more important in the density-matrix elements for the ground state than the spectroscopic $3d$ and $4d$ orbitals, which resulted in a dramatic reduction of the $W_2(p)$ strength at low momentum (<0.5 a.u.), and a corresponding increase in the cross section at high momentum ($p\sim 1.2$ a.u.).

Figure 3 shows on a linear scale the $3p$ and $3s$ momentum distributions obtained at 1500 eV for the ground-state and first-excited-state transitions, respectively. They are compared with the DWIA cross sections normalized as in Fig. 2(a). This again shows the excellent agreement between the data and the DWIA cross sections using the indicated spectroscopic factors.

The 1500-eV cross sections for the total $3s$ manifold and the remaining $3s$ satellites and the continuum up to 55 eV are shown in Fig. 4 compared with the DWIA cross section. It is evident that the momentum profiles

TABLE III. Comparison of spectroscopic factors for the ^2S manifold. Asterisk denotes decreases from 0.03 ± 0.01 at $p<0.2$ to 0.01 ± 0.01 at $p>0.5$ a.u.

Dominant configuration	Experiment (EMS)		Mitroy *et al.*[a] Overlap		Mitroy *et al.*[a] FSCI	Hibbert and Hansen[b] FSCI		Amusia and Kheifets[c] GF	Von Niessen[d] GF-ADC(4)	
	ε(eV)	S_f	ε(eV)	S_f	S_f	ε(eV)	S_f	S_f	ε(eV)	S_f
$3s3p^6$	29.24	0.55(1)	28.67	0.649	0.600	29.31	0.618	0.55	28.99	0.605
$3p^4 4s$	36.50	0.02(1)*	36.38	0.013	0.006	36.57	0.006		36.74	0.008
$3p^4 3d$	38.58	0.16(1)	38.65	0.161	0.142	38.84	0.112	0.20	39.08	0.135
$3p^4 4d$	41.21	0.08(1)	41.72	0.083	0.075	41.32	0.057	0.11	41.40	0.005
$3p^4 5d$	42.65					42.66	0.021	0.04	42.05	0.025
		0.08(1)		0.081	0.095					
$3p^4 6d$	43.40					43.44	0.009			
$Ar^{2+}+e$		0.12(1)		0.013	0.08		0.18			0.177

[a]Reference 5. [b]Reference 11. [c]Reference 4. [d]Reference 20.

for all of these transitions, except perhaps the one at 36.52 eV leading to the $(^1S)4s$ state, correspond to the $3s$ momentum profile, the relative cross sections being given by the spectroscopic factors.

Table II lists the spectroscopic factors for transitions belonging to the $^2S^e$ manifold. These are obtained from the measured energy spectra at different angles at 500, 1000, and 1500 eV. Quite clearly, within experimental errors, the spectroscopic factors are independent of incident energy and the momentum of the struck electron. The spectroscopic factors obtained in the present work are in excellent agreement with those recently obtained by McCarthy and Weigold[3] at 1000 eV, as well as those obtained in earlier less accurate work at a number of energies at $p \sim 0$.[1,17–22]

Table III lists the spectroscopic factors obtained in a number of many-body calculations. None of them adequately describes the data, although they do give the

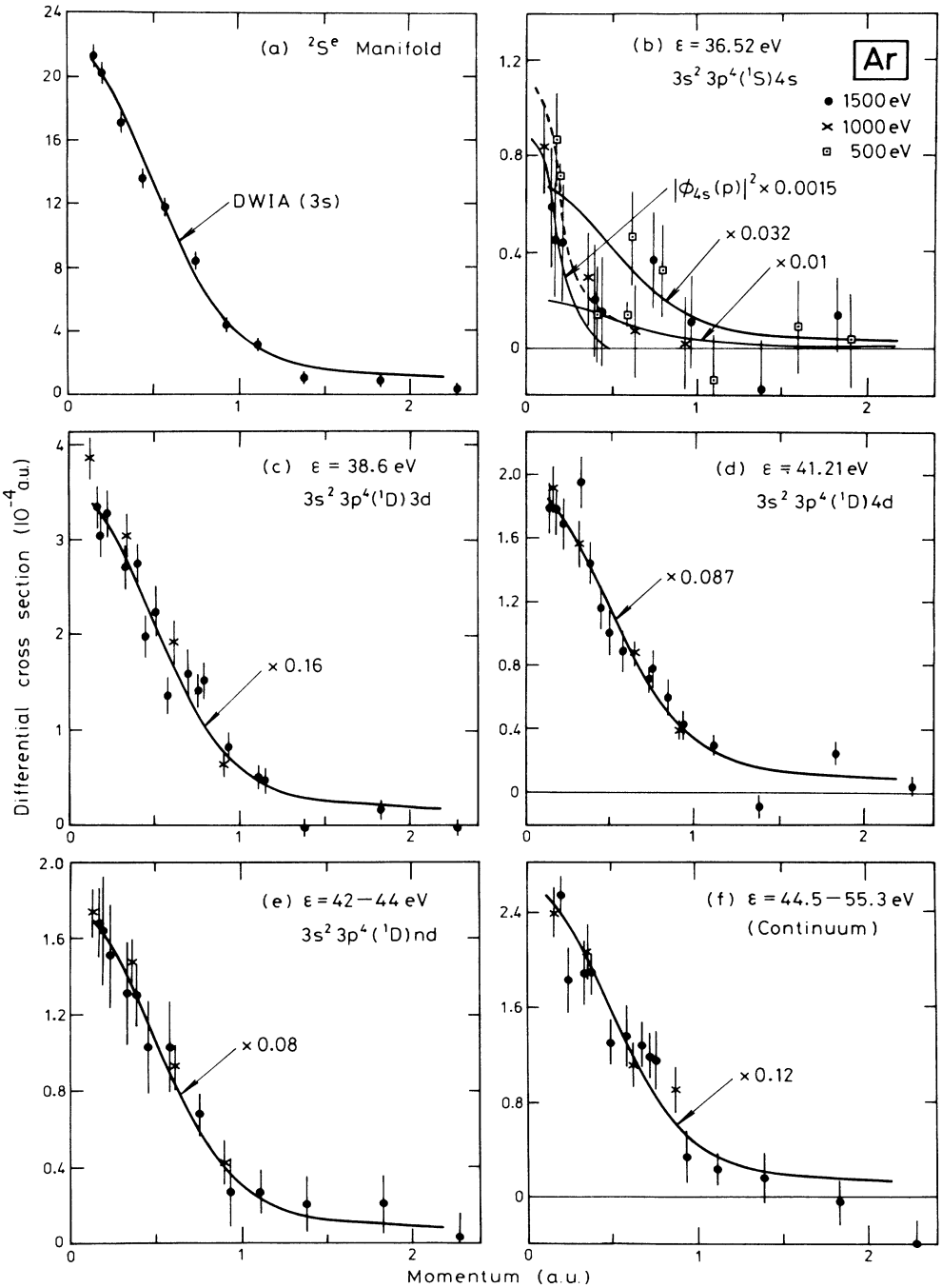

FIG. 4. Momentum profiles for the ^2S manifold and various satellites compared with the calculated $3s$ momentum profiles multiplied by the respective spectroscopic factors. For the $3s^2 3p^4 4s$ transition a $4s$ HF momentum profile multiplied by 0.0015 is also shown.

main features, i.e., a little more than half the strength belongs to the $3s3p^6$ state at 29.24 eV, with the next most prominent state being the $3s^23p^43d$ state at 38.60 eV. The most detailed calculation is that of Mitroy *et al.*,[5] who carried out a full calculation of the overlap function between the correlated target state and the correlated final states as shown in Eqs. (2) and (5). This is indicated by the column heading of overlap. The corresponding final-state CI calculation, which measures the percentage of $3s3p^6$ in the final state is also given. There is a significant difference between the full overlap calculation and the amplitude squared of the $3s3p^6$ configuration. The spectroscopic factor for the primary transition has increased from 0.60 to 0.65 in the full calculation, whereas the experimental value is 0.55. Two factors contribute to this increase in the calculation. The first is the coherent coupling between terms for the CI expansion of the atom and ion, and the second is the coherent addition of virtual orbital momentum-space wave functions with the 3*s* HF component. The experimental results suggest that the interference should be destructive rather than constructive. In the continuum region the full overlap calculation gives destructive interference, which reduces the spectroscopic strength of the continuum, again in disagreement with the measurements.

Hibbert and Hansen[11] carried out a CI calculation of only the ion states and not a full overlap calculation. Therefore their spectroscopic factors are only the square of the amplitude of the $3s3p^6$ component in the corresponding ion state. As Mitroy *et al.*[5] showed, inclusion of correlations in the ground state can lead to very significant changes in the distribution of the spectroscopic strength. It is therefore not surprising that this limited calculation is not in agreement with the measurements.

Amusia and Kheifets[4] obtain excellent agreement for the spectroscopic factor of the primary transition at 29.3 eV, but their Green's-function overlap calculation does not have sufficient flexibility to explain the richness of the observed ^2S manifold. They do, however, point out the difference between EMS and PES measurements, showing that the interpretation of PES results is very difficult and that PES intensities cannot be directly compared with calculated spectroscopic factors. They showed that in photoelectron spectroscopy, the spectroscopic factor for the lowest ion state is generally overestimated, while the spectroscopic factors for the other transitions are underestimated.

The calculations of Von Niessen[29] are based on the Green's-function technique, which takes into account both initial- and final-state correlations as well as relaxation effects. He used the ADC(4) approximation,[30] that is the algebraic diagrammatic expansion of the one-particle Green's function accurate to fourth order, and a $[12s9p6d1f]$-$(8s6p6d1f)$ Gaussian basis set. The general agreement with the data is quite reasonable.

Figure 4(b) shows the momentum distribution to the $3s^23p^4(^1S)4s$ ion state. The strength for this transition is due to three contributions. The first is the $3s3p^6$ component in the final-state wave function, which the CI calculations give to be approximately 0.6% (Table III); secondly, there is the effect of relaxation. The third contribution is due to initial-state correlation effects, mainly due to the $3s^23p^44s^2$ component in the ground-state wave function. This latter contribution, in the weak-coupling approximation, would lead to a 4*s* momentum distribution due to the knock-out of one of the 4*s* electrons. The 4*s* momentum distribution is much narrower than the 3*s* and (for equal occupancy) has much greater value at zero momentum than the 3*s*. The distribution in Fig. 4(b) shows an enhancement at low momentum which could indeed be due to the 4*s* component. The shape of the momentum distribution is significantly different from the 3*s* one if the points with poor statistics above $p \sim 0.6$ a.u. are neglected. This is particularly obvious in the two most accurate data points at 500 eV and $p \sim 0.2$ and 0.6 a.u. Mitroy *et al.*[5] find that the influence on the $l=0$ manifold momentum profile $W_s(p)$ is quite small, although due to the large value of $\phi_{4s}(p)$ at the origin the total ^2S strength is increased by some 4% at $p=0$ dropping to the HF value at $p \sim 0.3$ a.u.

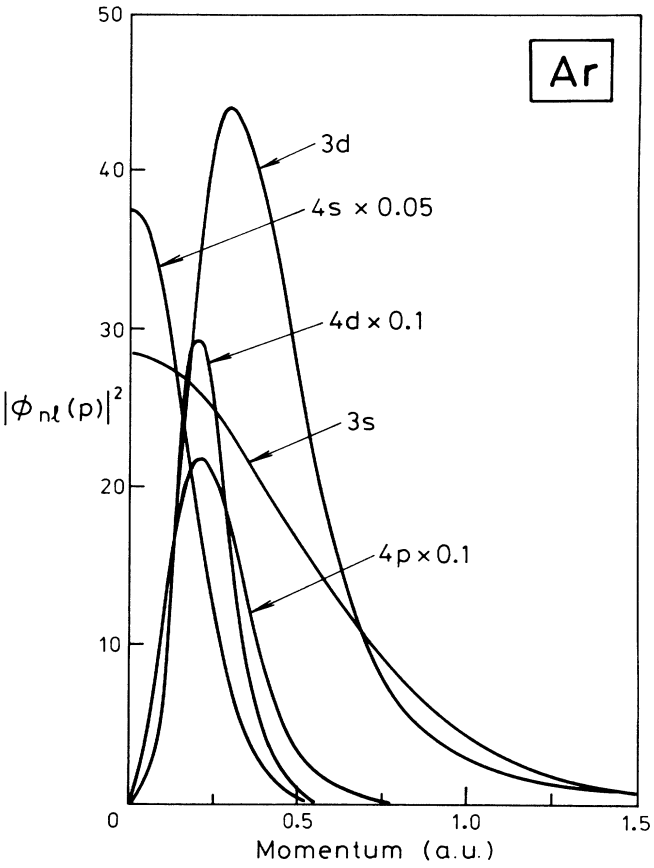

FIG. 5. Calculated HF momentum profiles for the Ar 3*s*, 4*s*, 4*p*, 3*d*, and 4*d* orbitals.

The momentum distributions for the 4*s* as well as the 4*p*, 3*d*, and 4*d* spectroscopic orbitals are compared with the 3*s* HF momentum probability distribution in Fig. 5.[28] The 4*s* momentum distribution is approximately 25 times that of the 3*s* at $p=0$, but it is much more sharply

peaked. In Fig. 4(b) we have included for comparisons a $4s$ cross section amounting to 4% of the total $3s$ cross section at $p=0$, the maximum permitted by the calculation of Mitroy *et al.*[5] This corresponds to a $4s$ strength of 0.0015. Also shown is a $3s$ contribution of 0.01, as well as the sum of the two. This is in excellent agreement with the data, in particular the two most accurate measurements at 500 eV at $p\sim 0.2$ and 0.6. We have added the two contributions coherently, but obviously any phase between the two contributions is possible. The $3s3p^6$ component in this state is very likely of the order of 0.01, in good agreement with the calculations.

The momentum profile for the continuum up to 55.3 eV is shown in Fig. 4(f). Clearly, the continuum strength must belong primarily to the $^2S^e$ manifold, the $^2P^o$ contribution being negligible. The continuum was therefore assigned to the $^2S^e$ strength in Figs. 2 and 4(a) and in Tables II and III. Although Fig. 1 and similar separation energy spectra at 1000 and 1500 eV show that the continuum strength has all but disappeared by 55 eV, a very small contribution above this energy cannot be ruled out. The continuum spectroscopic strength in Table II must therefore be considered a lower bound, any extra strength in the continuum would lower the other relative spectroscopic factors accordingly.

Figure 6 shows the momentum distributions to final states that do not belong to the $^2S^e$ manifold. The first is the state at 34.20±0.08 eV. This has the assignment $3s^23p^4(^1D)4s\ ^2D$.[25] This state can only be excited through d-wave correlations in the ground state of the neutral argon atom. The observed momentum distribution shows a maximum at $p\sim 0.25$ a.u., a minimum at $p\sim 0.4$ a.u., and a broad secondary maximum at $p\sim 0.7$ a.u. The $^2D^e$ manifold momentum distribution calculated by Mitroy *et al.*[5] is also shown in Fig. 6(a) and is marked CI ($l=2$). It is multiplied by a factor of 2 for ease of comparison at low momentum. Clearly this CI calculation underestimates the height of the small momentum

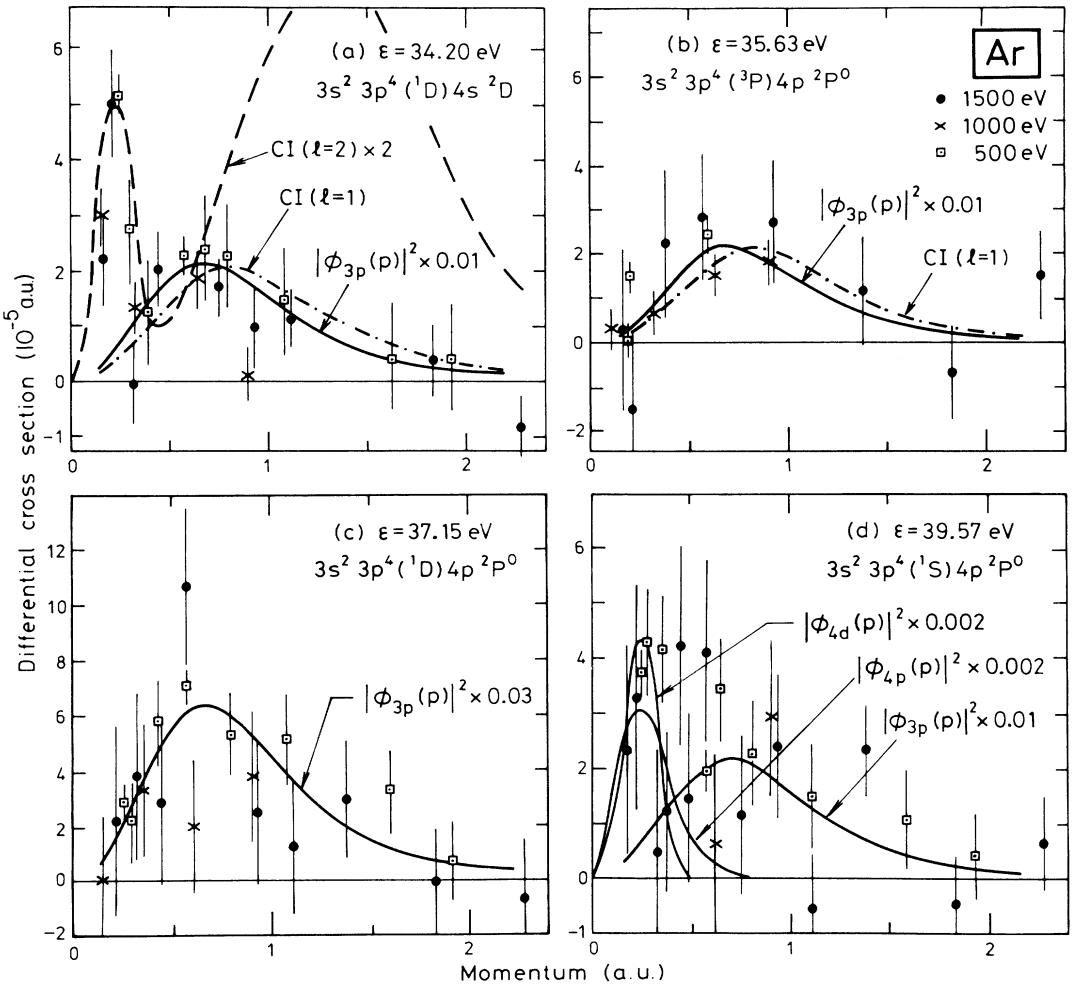

FIG. 6. Measured momentum profiles to final states at 34.2, 35.6, 37.15, and 39.6 eV compared with several calculated distributions. The factors following the $3p$ calculated distributions are $3p$ spectroscopic factors. The CI ($l=2$) distribution is the total ^2D manifold distribution obtained by Mitroy *et al.* (Ref. 5). The CI ($l=1$) distributions are 0.67 of the total $^2P^o$ satellite distribution obtained by Mitroy *et al.* The $4d$ and $4p$ distributions are the HF spectroscopic Ar $4d$ and $4p$ momentum distributions with their respective scaling factors.

peak and overestimates the contribution at high momentum. Mitroy *et al.* found that the dominant contribution of the correlation energy came from "correlating" pseudonatural orbitals (denoted by a bar) rather than the spectroscopic orbitals. The contracted $\bar{3}d$ orbital, which was localized in the same region of space as the $3s$ and $3p$ orbitals, is much more important in its density matrix elements for the ground state than the much more diffuse spectroscopic $3d$ and $4d$ orbitals. Figure 5 shows that in momentum space the spectroscopic orbitals are peaked at low momentum ($p \sim 0.25$ a.u.), whereas the contracted $\bar{3}d$ orbital is peaked at high momentum ($p \sim 1.2$ a.u.). Clearly our data show that the spectroscopic $3d$ and $4d$ orbitals are more important than given by the calculation of Mitroy *et al.*, and that they probably overestimate the large momentum components due to the $\bar{3}d$ orbital. If the intensity of the low momentum peak is attributed to a ground-state $3s^2 3p^4(^1D)4s3d$ configuration it would require a 3% admixture (see Fig. 5) in order to explain the cross section. A $3s^2 3p^4(^1D)4s4d$ configuration would require a CI contribution of only 0.4%. The shape of the low-momentum peak is given very well by the $4d$ momentum distribution, and not so well by the $3d$ (see Fig. 5).

Dyall[27] has also carried out a CI calculation of the ground state including double excitations of the form $(nl)^2$, but included only the spectroscopic $3d$ and $4d$ orbitals (as well as other nl orbitals up to $nl=5p$). He found that the major interaction in the Ar ground state involved the $3p^4 3d^2$ and $3p^4 4d^2$ configurations, which contributed 1.2% and 0.5% of the correlated wave function, respectively. According to this calculation the total d-wave intensity should be approximately 9% of the total $3s$ intensity at 0.25 a.u. (Ref. 27). Thus the total cross section for the $^2D^e$ manifold should be of the order of 1.7×10^{-4} a.u. at $p=0.25$ a.u. This is 3.4 times higher than the strength observed for the 34.20-eV transition. Since Dyall included only the $3d$ and $4d$ spectroscopic orbitals, he does not predict any detectable cross section above $p \sim 0.5$ a.u., which is in disagreement with the data. The possibility of some $^2P^o$ contribution in this energy range at large momentum must be explored since there is a state of ^2P symmetry at 34.50 eV, namely, the $3s^2 3p^4(^3P)3d$ state. This state could be largely discounted on the basis of separation energy, the fit to the data at this energy being unacceptable. It is therefore extremely unlikely that this state accounts for a significant part of the observed strength [Fig. 6(a)], and certainly cannot account for any of the low-momentum strength. Nevertheless, in Fig. 6(a) we include two calculations of the ^2P manifold momentum distribution. The first is simply 0.01 times the $3p$ HF DWIA cross section (solid line) and the second is 0.67 of the total $^2P^o$ satellite intensity, marked CI ($l=1$), calculated by Mitroy *et al.* in their full overlap calculation by subtracting the calculated distribution for the $3s^2 3p^5$ ground-state transition from the total $^2P^o$ manifold distribution. There is a small difference in shape between the HF and CI calculations due to the effect of initial-state correlations. Both describe the high-momentum tail quite well.

The next transition at 35.63 eV leading to the $3s^2 3p^4(^3P)4p\ ^2P^o$ state has clearly a $3p$ momentum profile [Fig. 6(b)], although the transition is very weak. It has again been compared with 0.01 of the HF momentum distribution and 0.67 of the $^2P^o$ total satellite momentum distribution calculated by Mitroy *et al.* Figure 6(c) shows the momentum distribution for the transition leading to the $3s^2 3p^4(^1D)4p\ ^2P^o$ state at $\varepsilon=37.15$ eV. This again is clearly $3p$ in character and has a considerably larger cross section, approximately 3% of that for the ground-state transition. There is no evidence for excitation of the $3s^2 3p^4(^1D)3d$ state at 37.18 eV, there being no low-momentum components as expected from a $3d$ transition [Figs. 5 and 6(a)].

Figure 6(d) shows the momentum distribution at $\varepsilon=39.6$ eV. The obvious candidate for the final state is the $3s^2 3p^4(^1S)4p\ ^2P^o$ ion state at 39.57 eV. For comparison the HF $3p$ momentum profile has been included in the figure. Clearly there is some excess intensity at low momentum. This could be due to some $4p$ component in the overlap function or it could be due to a transition to another final state. The only other candidate is the $3s^2 3p^4(^3P)4d\ ^2D$ state at 39.64 eV. Indeed, the momentum distribution in Fig. 6(d) is very similar to that observed in the ^2D transition shown in Fig. 6(a), given the large error bars on some of the data points. The most accurate data, namely, the 500-eV points at $p \sim 0.22$ and 0.6 a.u., are strikingly similar in Figs. 6(a) and 6(d) and certainly are not consistent with the $3p$ momentum profile. It seems likely therefore that a considerable part of the observed intensity at 39.6 eV is due to the ^2D final state. There could also be some $4p$ contribution, the p momentum profile being very similar to that of the $4d$ (see Fig. 5).

The spectroscopic factors obtained by us for the $^2P^o$ manifold are given in Table IV where they are also compared with several calculations and the photoelectron re-

TABLE IV. Relative spectroscopic factors for the $^2P^o$ manifold of Ar II determined from the relative $(e,2e)$ cross sections at 500, 1000, and 1500 eV at $p \sim 0.7$ a.u. compared with several calculated values.

Dominant configuration	ε (eV)	Present EMS	Mitroy *et al.*[a] Full overlap ($P=0.7$)	FSCI	Von Niessen[b] GF-ADC(4)	Dyall and Larkin[c] HF (relax)	Dyall and Larkin[c] FSCI	Svenson *et al.*[d] (γ,e)
$3s^2 3p^5$	15.76	0.95±0.02	0.972	0.916	0.929			≤ 0.95
$3s^2 3p^4(^3P)4p$	35.60	0.01±0.005	0.002	0.001		0.011	0.002	0.004
$3s^2 3p^4(^1D)4p$	37.15	0.03±0.01	0.013	0.014	0.025	0.007	0.012	0.022
$3s^2 3p^4(^1S)4p$	39.57	0.01±0.005	0.002	0.002		0.0015	0.003	0.009

[a]Reference 5. [b]Reference 29. [c]Reference 26. [d] Reference 31.

sults of Svenson *et al.*[31] The calculations include some with the full overlap function and some in which only relaxation and final state configuration interaction (FSCI) were included. The full overlap spectroscopic factors of Mitroy *et al.* are obtained at $p=0.7$ a.u. The Green's-function calculation of von Niessen[29] gives a significantly lower pole strength for the ground-state transition than the CI calculation of Mitroy *et al.* The experimental value of 0.95 ± 0.01 is in between the two theoretical values. In general, the calculations for the $^2P^o$ manifold are broadly in agreement with the experimental results, although the calculated pole strengths for the satellite lines are rather smaller than the measured ones. It is interesting to note that Wijesundera and Kelly,[32] who use many-body perturbation theory, which includes both initial- and final-state correlation effects, find significantly larger cross sections at high photon energies for the three $4p\ ^2P^o$ satellite transitions than do Dyall and Larkins.[26] Given the experimental errors, the agreement between the EMS and PES (Ref. 31) results is very good.

V. CONCLUSIONS

The distorted-wave impulse approximation gives a complete description of the shapes and relative magnitudes of the 1500-eV noncoplanar symmetric $Ar(e,2e)Ar^+$ differential cross sections leading to the $3s^23p^6(^2P^o)$ Ar^+ ground state and to the $^2S_{1/2}$ manifold of final states. The shapes of the cross sections are very well described by the HF $3p$ and $3s$ momentum probability distributions out to about 1.5 and 1.2 a.u. of momentum, respectively. The momentum profiles to a whole series of final states as well as to the $Ar^{2+}+e$ continuum have been measured, and the transitions allocated to the $^2S^e$, $^2P^o$, and $^2D^e$ manifolds. Data at 500 and 1000 eV have also been included. The $^2S^e$ transitions are very well described by the HF $3s$ wave function, except for the low-intensity transition to the $3s^23p^4(^1S)4s$ ion state at 36.5 eV, which shows evidence of $4s$ contributions due to $4s^2$ configurations in the Ar ground state. The spectroscopic factors or pole strengths for the ^2S manifold are found to be independent of energy in the range 500–1500 eV and independent of momentum within experimental error in the range 0–1.9 a.u. There is good evidence that the spectroscopic factor for the $3s^23p^44s$ transition varies a little with momentum, decreasing from a value of about 0.30 ± 0.005 at $q\sim0$ to 0.010 ± 0.005 at $p\sim0.5$ a.u. This is due to initial-state correlations.

We have observed, for the first time, transitions belonging to the ^2D manifold. These can only occur if there are d-wave correlations in the Ar ground state. The most prominent $^2D^e$ transition is to the $3s^23p^4(^1D)4s$ state at 34.20 eV. The momentum distribution to this state is very interesting. It has a narrow peak at $p\sim0.25$ a.u., which is to be expected from the diffuse (in coordinate space) spectroscopic $3d$ and $4d$ orbitals. However, after a minimum at $p\sim0.5$ a.u. the cross section shows a second maximum at $p\sim0.7$ a.u. at about half the intensity of the small momentum peak. This high-momentum component is not expected if only the spectroscopic nl orbitals contribute to the Ar ground-state correlations. A CI calculation by Mitroy *et al.*, which includes correlating pseudonatural $\overline{3d}$ orbitals contracted to the same space as the $3s$ and $3p$ orbitals, found that the high-momentum component should dominate due to the effect of the $\overline{3d}$ orbital. Although the experiment does show "nonspectroscopic" high-momentum components, their effect is overestimated in the CI calculation of Mitroy *et al.*

The transition at $\varepsilon=39.6$ eV also has a very similar momentum distribution to that for the $3s^23p^4(^1D)4s\ ^2D$ state. This could be due to excitation of the $3s^23p^4(^3P)4d\ ^2D$ ion state at 39.64 eV. Some of the cross section is also probably due to the excitation of the $3s^23p^4(^1S)4p\ ^2P^o$ ion state at 39.57 eV. Although the low-momentum region cannot be explained by a $3p$ ionization process, there could be a $4p$ contribution from the $3s^23p^4(^1S)4p^2$ component in the Ar ground state. The $4p$ momentum distribution is very similar to the $4d$ distribution.

There are two definite $^2P^o$ transitions in addition to the dominant ground-state transition. These are to the $3s^23p^4(^3P)4p$ and $3s^23p^4(^1D)4p$ ion states at 35.63 and 37.15 eV, respectively. Both transitions have the $3p$ momentum distribution, but the spectroscopic factors are very small, being 0.01 and 0.03, respectively. The spectroscopic factor for the ground-state transition is almost unity, having a value of 0.95 ± 0.01. The observed spectroscopic factors in the $^2P^o$ manifold are in very good agreement with a number of many-body calculations.

One interesting aspect of this work is that it shows the importance of collective quadrupole coupling in the core due to correlation effects. This is not only the case in the final-state correlations in the $^2S^e$ manifold where $3s^23p^4(^1D)$ core coupling is totally dominant, but also in the collective many-body effects in the ground state, where again $3s^23p^4(^1D)nln'l'$ configurations are dominant. It therefore seems essential that the many-body calculation of atomic structure should take care in treating the quadrupole-core excitations accurately.

ACKNOWLEDGMENTS

We are grateful to the Australian Research Council for financial support of this work. We are also indebted to Professor W. von Niessen for providing us with the results of his Green's-function calculation.

[1] I. E. McCarthy and E. Weigold, Phys. Rep. **27C**, 275 (1976).
[2] J. Mitroy, I. E. McCarthy, and E. Weigold, J. Phys. B **18**, L91 (1985).
[3] I. E. McCarthy and E. Weigold, Phys. Rev. A **31**, 160 (1985).
[4] M. Ya Amusia and A. S. Kheifets, J. Phys. B **18**, L679 (1985).
[5] J. D. Mitroy, K. A. Amos, and I. Morrison, J. Phys. B **17**, 1659 (1984).
[6] H. Smid and J. E. Hansen, J. Phys. B **14**, L811 (1981).
[7] J. E. Hansen, Comments At. Mol. Phys. **12**, 197 (1982).
[8] H. Smid and J. E. Hansen, J. Phys. B **16**, 3339 (1983).

[9]H. Smid and J. E. Hansen, Phys. Rev. Lett. **52**, 2138 (1984).
[10]H. Smid and J. E. Hansen, J. Phys. B **18**, L97 (1985).
[11]A. Hibbert and J. E. Hansen, J. Phys. B **20**, L245 (1987).
[12]C. E. Brion, K. H. Tan, G. M. Bancroft, Phys. Rev. Lett. **56**, 584 (1986).
[13]C. E. Brion, A. O. Bawagan, and K. H. Tan, Chem. Phys. Lett. **134**, 76 (1987).
[14]H. Kossmann, B. Krässig, V. Schmidt, and J. E. Hansen, Phys. Rev. Lett. **58**, 1620 (1987).
[15]S. Svensson, K. Helenelund, and U. Gelius, Phys. Rev. Lett. **58**, 1624 (1987).
[16]D. P. Spears, H. J. Fishbeck, and T. A. Carlson, Phys. Rev. A **9**, 1603 (1974).
[17]E. Weigold, S. T. Hood, and P. J. O. Teubner, Phys. Rev. Lett. **30**, 475 (1973).
[18]S. T. Hood, I. E. McCarthy, P. J. O. Teubner, and E. Weigold, Phys. Rev. A **9**, 260 (1974).
[19]I. E. McCarthy and E. Weigold, Rep. Prog. Phys. **51**, 299 (1988).
[20]E. Weigold and I. E. McCarthy, Adv. Atom. Mol. Phys. **14**, 127 (1978).
[21]K. T. Leung and C. E. Brion, Chem. Phys. **82**, 87 (1983).
[22]J. F. Williams, J. Phys. B **11**, 2015 (1978).
[23]J. P. D. Cook, I. E. McCarthy, A. T. Stelbovics, and E. Weigold, J. Phys. B **17**, 2339 (1984).
[24]J. P. D. Cook, I. E. McCarthy, J. Mitroy, and E. Weigold, Phys. Rev. A **33**, 211 (1986).
[25]C. Moore, *Atomic Energy Levels,* Natl. Bur. Stand. (U.S.) Circ. No. 467 (U.S. GPO, Washington, D.C. 1949), Vol. 1.
[26]K. G. Dyall and F. P. Larkins, J. Phys. B **15**, 219 (1982).
[27]K. G. Dyall, Ph.D. thesis, Monash University, 1980.
[28]E. Clementi and C. Roetti, At. Nucl. Data Tables **14**, 177 (1974).
[29]W. von Niessen (private communication).
[30]O. Walter and J. Schirmer, J. Phys. B **14**, 1237 (1983).
[31]S. Svenson, B. Erikson, N. Martensson, G. Wendin, and U. Gelius, J. Elec. Spectrosc. **47**, 327 (1988).
[32]W. Wijesundera and H. P. Kelly, Phys. Rev. A **39**, 634 (1989).